Methodology for Fast Calculation of Impedance Matrix of Power Transformers for High Frequency Transient Studies

Guillermo A. Diaz, Enrique E. Mombello, Jhon Perez G. and Hans K. Høidalen

***Abstract*—Power transformers are exposed to a variety of disturbances that may jeopardize their lifespan and the safe operation of the power system. The transient behavior of the transformer can be assessed by means of white-box models. The main prerequisite for the development of the white-box model is the frequency-dependent impedance matrix of the transformer. The main obstacle that restricts the use of white-box models at industrial level lies in the computation of the impedance matrix, since this calculation requires magnetic-field numerical simulations, which demand disproportionate calculation times when performed with traditional techniques such as the finite element method (FEM). That is why this paper proposes a new methodology for the fast calculation of the frequency-dependent impedance matrix of power transformers, which produces matrices suitable for the development of accurate white-box models. The proposed methodology was validated on a real 50 MVA transformer. Two white-box models were elaborated, one from the impedance matrix calculated with the proposed method and other using the matrix obtained with FEM. Excellent agreement was found between the transient response measurements and the response obtained with both models, however the proposed method reported a drastic reduction in computation time compared to FEM.**

***Index Terms*—Power transformer, electromagnetic transients, impedance matrix, white-box model, Mesh-Free Method, FEM.**

I. Introduction

The transformer is undoubtedly one of the most important elements of the power system due to its high replacement cost and the serious operational problems that arise when a unit fails. This is why the transformer must be designed to withstand various disturbances from the network to which it may be subjected during its operation. Among the most studied disturbances are overvoltages caused by atmospheric discharges and those due to switching in the power network. Although transformers are designed taking into account the existence of these disturbances and are tested to determine their withstand to these phenomena, cases of failure have been reported in transformers that had successfully passed these tests. That is why a CIGRE working group [1], [2] was created to determine the possible causes of failure in these situations and to formulate strategies to prevent or at least mitigate the damage to the power transformer.

Guillermo A. Diaz and Jhon Perez G. are with the Department of Electrical Engineering, La Salle University, Bogota, Colombia, e-mail: guandiaz@unisalle.edu.co (see https://www.lasalle.edu.co/).

Enrique E. Mombello is with CONICET-National University of San Juan.

Hans K. Høidalen is with the Department of Electric Power Engineering, Norwegian University of Science and Technology, Trondheim, Norway.

One of the most important conclusions of the CIGRE A2/C4.39 working group is that these faults can only be explained if the phenomenon of resonance produced by the interaction of the network with the transformer is considered. As a consequence, there is a need to create new and more detailed high frequency models of the power transformer in order to correctly represent this type of transient phenomena. In response to this need, a state-space white-box model suitable for accurate modeling of transformer interaction with the power network under high frequency transient phenomena has been proposed recently in [3]. The main advantage of this model is its ability to consider the frequency dependence of the inductive impedances of the transformer. This is of primary importance to adequately represent the damping, making the model suitable to evaluate the severity of transient phenomena even under resonant conditions. This model has been developed in the framework of a more recent working group identified as JWG CIGRE A2/C4.52.

The methodology proposed in [3] to obtain the white box model of the power transformer can be summarized as follows: *a*. Subdivision of the transformer into m branches and preparation of the geometrical model for magnetic and electric field calculations. *b*. Calculation of the impedance matrix (inductive-resistive) $\mathbf{Z}(\omega)$ as a function of frequency at a set of the selected frequencies. The impedance matrix is a hypermatrix of size $m \times m \times n_f$ where n_f is the total number of frequencies to be considered. *c*. Robust fitting of the partial fraction expansion from the matrix $\mathbf{Z}(\omega)$ using vector fitting and PSO (Particle Swarm Optimization). *d*. Calculation of the capacitance and conductance matrix. *e*. Synthesis of the state-space model.

Once the model has been obtained, it is possible to calculate the transformer response to various transient phenomena using EMTP software or by means of the numerical solution of the differential equation system of the state space model. Despite the high accuracy of the state-space model, there are still some difficulties to overcome before these models can be adopted by the industry.

In the methodology to obtain the white box model of the transformer described above, the most computationally demanding step corresponds to the calculation of the impedance matrix as a function of frequency. This is because a number of $m \cdot n_f$ magnetic simulations must be performed, and for each of them the induced voltage in each of the branches has to be calculated. Due to the complexity of the transformer geometry this calculation is usually performed using the Finite Element

Method (FEM) [4].

As a result of the large number of simulations to be performed and the fact that FEM subdivides the entire problem domain, the calculation of the impedance matrix may take an excessive amount of time to complete. Although it is possible to use a computer cluster to reduce computational time as reported in [5], not all transformer manufacturers currently have such computational resources, therefore research on new methods to speed up these calculations is of great value to the industry.

This is why a new approximate method is needed to compute the frequency-dependent impedance matrix with a more reasonable calculation time and preserving the suitability of the white-box model to calculate electromagnetic transients. Because of this, the main purpose of this work is the development of a methodology for a faster calculation of the power transformer impedance matrix taking into account relevant factors in high frequency modeling such as the effect of the core on the leakage flux and the frequency dependence of losses in materials such as in the copper of conductors and in the iron core.

The calculation of impedance matrix parameters has been studied for decades in previous works. One of the first works addressing this subject is the one by Wilcox et al [6]. In this work an analytical formula is proposed that allows the determination of the impedances of the transformer windings considering the frequency dependence of these parameters. The effect of the iron core was considered, nevertheless the skin and proximity effect were not taken into account.

Subsequently, De Leon proposes in [7] a methodology for calculating transformer stray inductances using the image method without consideration of losses. In a subsequent work De Leon includes the frequency dependence of the losses [8].

One of the most important advances in this field was made by Moreau in [9] introducing the analytical formulas for the calculation of the complex permeabilities needed for equivalent modeling of conductors in 2D static FEM simulations. This allowed the calculation of the impedance matrix without the need to perform full-eddy simulations.

In this same vein, Bjerkan obtains the parameters of a real 20 MVA transformer from 2D axisymmetric FEM simulations using the proprietary software called SUMER [10]. In [11] it is reported that using SUMER the time to obtain a matrix at a single frequency may take from 20 minutes to a few hours depending on the complexity of the transformer.

After Moreau's work [9], the use of FEM for impedance matrix calculation has become virtually standard in the magnetic modeling of high-frequency power transformers [12], [13]. Despite this, no research has been found that directly addresses the problem of the efficient calculation of the impedance matrix, which is the main motivation for the present research work.

The main contributions of this work are: *a.* A mesh-free model is proposed for quasi-stationary magnetic modeling of the power transformer through the combined use of surface currents and complex permeabilities. *b.* From matrices derived from the magnetic model, a novel and efficient methodology for the calculation of the impedance matrix is proposed. *c.* An excellent agreement was found between the results obtained with the proposed methodology and measurements in a real 50 MVA transformer. *d.* The calculation time of the proposed methodology reported a substantial improvement with respect to the calculation time using FEM.

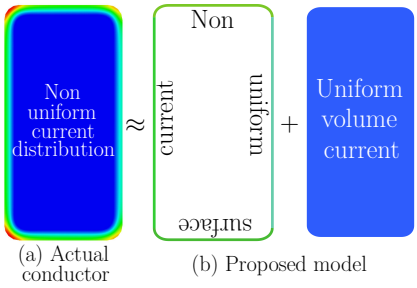

Fig. 1. Proposed equivalent model of conductors.

II. Description of the Proposed Model

In order to obtain the impedance matrix, it is essential to have a suitable equivalent magnetic model of the transformer. Some of the difficulties encountered with FEM in meeting this objective are described and how these issues are overcome with the proposed model.

A. Equivalent magnetic model of conductors

Fig. 1(a) shows the current distribution of a typical conductor at a frequency of 100 kHz. This single wire was taken from a larger arrangement of conductors in a power transformer winding. The final current density distribution is determined by the skin effect and the proximity effect. As the frequency increases the current density exhibits a strong tendency to increase near the outer boundary of the conductor due to the skin effect. This means that beyond certain frequencies, the current distribution in the conductors is similar to that shown in Fig. 1(a).

As can be seen, this is a non-uniform current distribution on the conductor cross-section, although it can also be seen that the current density in the interior of the conductor tends to be uniform, while the current density near its surface tends to be non-uniform. This current distribution suggests the possibility of approximately representing the conductor by superimposing a non-uniform surface current on its surface, and a uniform current distribution in its interior as shown in 1(b).

Fig. 2(a) shows the finite element mesh produced by Ansys Maxwell software at 100 kHz on the same conductor. As can be seen, there is an increased element density near the surface of the conductor in order to capture the non-uniformity in the current distribution. This is a major problem, since a power transformer can be designed with thousands of conductors, thus producing a mesh with millions of triangular elements, which makes the problem almost impossible to solve with traditional computational resources.

To overcome some of these problems, it is possible to use the concept of complex permeability in conjunction with FEM, thus avoiding full eddy simulations with ultra fine meshes at high frequencies. However, the internal subdivision of

conductors (in addition to the core and the free space) is still necessary, persisting the problem of the huge size of the equations system.

In order to considerably improve computational efficiency without significantly compromising the accuracy of the solution, a new equivalent conductor model has been proposed as shown in Fig. 2(b). This equivalent model consists of a set of surface elements with linear surface current density distribution surrounding the outer boundary of the conductor. Regarding the internal region of the conductor, a uniform volume current distribution has been placed. Both surface currents and volume currents are unknown at the beginning of the solution process, therefore it is necessary to rely on a suitable representation compatible with the proposed conductor model to be able to determine the unknown quantities. *This suitable representation will be achieved through the combination of the complex permeability model with the equivalent model of magnetic materials using surface currents*.

The main idea of the complex permeability model is to replace an anhysteretic solid conductor with real isotropic permeabililty $\mu \approx \mu_0$ by a hysteretic material with complex anisotropic permeability $\underline{\boldsymbol{\mu}} = \text{diag}(\underline{\mu}^{(r)}, \underline{\mu}^{(z)})$ that leads to the same active and reactive power as the solid conductor [9]. Since in the complex permeability model the current density is uniform inside the conductor, this allows the interior of the conductor to be represented by a uniform volume current as shown in Fig. 2(b).

Regarding the equivalent model of magnetic materials using surface currents, the fundamental idea behind this technique is to replace a solid magnetic material by an equivalent surface current distribution such that the magnetic field of the new arrangement (using surface currents) is equivalent to that of the original one. Assuming initially a magnetic material with real and isotropic relative permeability μ, its equivalent model with surface currents must satisfy the following relationship on the boundary that separates the magnetic material from the free space [14]

$$\hat{\boldsymbol{n}} \times \vec{\underline{\boldsymbol{H}}} = \gamma \cdot \vec{\underline{\boldsymbol{K}}} \tag{1}$$

where $\vec{\underline{\boldsymbol{H}}} = H_r \hat{\boldsymbol{r}} + H_z \hat{\boldsymbol{z}}$ is the magnetic field strength in A/m, $\vec{\underline{\boldsymbol{K}}} = \underline{k}\hat{\boldsymbol{\phi}}$ is the surface current in A/m, $\hat{\boldsymbol{n}} = n^{(r)}\hat{\boldsymbol{r}} + n^{(z)}\hat{\boldsymbol{z}}$ is the normal vector to the surface always pointing towards the free

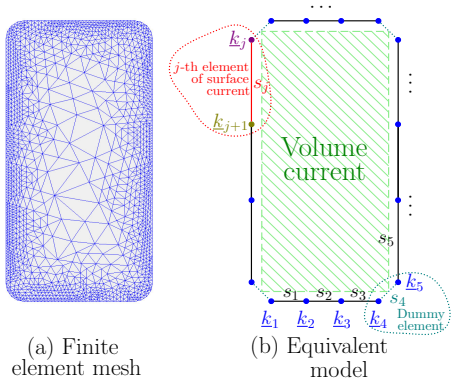

(a) Finite element mesh (b) Equivalent model

Fig. 2. (a) Finite element mesh of a typical conductor @ 100 kHz. (b) Equivalent model of a typical conductor using volume and surface currents.

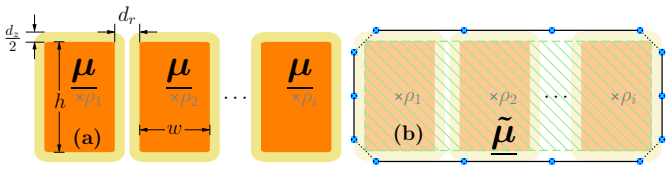

Fig. 3. (a) Group of conductors with the same properties and dimensions. (b) Winding segment with homogenized complex permeability.

space, $\gamma = (1/2)(1+\mu)/(1-\mu)$ is a constant that depends on the relative permeability of the magnetic material and $\hat{\boldsymbol{r}}, \hat{\boldsymbol{z}}$ are unit vectors in radial and axial direction respectively. In general, all underlined quantities represent complex numbers and axisymmetric geometry will be considered in this paper. The complete derivation of (1) from the Ampere's law can be found in [14]. As can be seen in (1), the material constant γ is real and isotropic, therefore this expression needs to be extended for the complex anisotropic case which is achieved as follows

$$\hat{\boldsymbol{n}} \times \vec{\underline{\boldsymbol{H}}} = \mathbf{1}_2^T \cdot \left\{ (\boldsymbol{\Upsilon} \cdot \boldsymbol{J}_2) \cdot \boldsymbol{\eta}^{\circ 2} \right\} \cdot \vec{\underline{\boldsymbol{K}}} \tag{2}$$

where $\boldsymbol{\Upsilon} = \text{diag}(\underline{\gamma}^{(r)}, \underline{\gamma}^{(z)})$ is a tensor with the complex constants of the magnetic material in radial and axial directions, $\boldsymbol{\eta} = [n^{(r)}; n^{(z)}]$ is a column vector with normal vector components, $\boldsymbol{J}_2 = [0, 1; 1, 0]$ is the exchange matrix of order 2, $\mathbf{1}_2$ is the ones vector of size 2×1, T represents the transpose operation and $\circ 2$ denotes the 2nd Hadamard power. The magnetic material constants in each direction are given by

$$\underline{\gamma}^{(r)} = (1/2)(1+\underline{\mu}^{(r)})/(1-\underline{\mu}^{(r)})$$
$$\underline{\gamma}^{(z)} = (1/2)(1+\underline{\mu}^{(z)})/(1-\underline{\mu}^{(z)})$$

where $\underline{\mu}^{(r)}$ and $\underline{\mu}^{(z)}$ are the relative complex permeabilities in radial and axial direction respectively. According to the complex permeability model [9], the relative complex permeabilities can be calculated using

$$\underline{\mu}^{(r)} = \frac{\mu_m}{\mu_0 h'} \cdot \frac{\sinh h' + \sin h' - \underline{j}\,(\sinh h' - \sin h')}{\cosh h' + \cos h'} \tag{3}$$

$$\underline{\mu}^{(z)} = \frac{\mu_m}{\mu_0 w'} \cdot \frac{\sinh w' + \sin w' - \underline{j}\,(\sinh w' - \sin w')}{\cosh w' + \cos w'} \tag{4}$$

where $h' = h/\delta_m$, $w' = w/\delta_m$, $\underline{j} = \sqrt{-1}$, h and w are the conductor's height and width respectively. $\delta_m = 1/\sqrt{f\mu_m\sigma_m\pi}$ is the skin depth of the material and f is the frequency of the simulation in Hz. μ_m and σ_m are the absolute permeability and electric conductivity of the actual material.

B. Equivalent magnetic model of winding segments

A power transformer can easily be composed of several thousand conductors, making the representation of all of them a rather difficult problem to solve in computational terms. A common practice to simplify the problem is to group the conductors into segments that are magnetically equivalent to the original set of conductors. This grouping is usually referred to in the literature as *homogenization*. At the same time, a group of segments constitutes a branch. The following

expressions are used to calculate the homogenized relative complex permeabilities of a winding segment [9], [15]

$$\underline{\tilde{\mu}}^{(r)} = \frac{d_r + w}{d_r + \frac{w(h+d_z)}{\underline{\mu}^{(r)} h + d_z}}, \underline{\tilde{\mu}}^{(z)} = \frac{\frac{h+d_z}{d_r} + \frac{d_z}{w} + \frac{h}{\underline{\mu}^{(z)} w}}{\frac{w+d_r}{d_r}\left(\frac{d_z}{w} + \frac{h}{\underline{\mu}^{(z)} w}\right)} \quad (5)$$

where $d_z/2$ is the thickness of the insulating paper of the conductor and d_r is the radial spacing between conductors (metal to metal) as shown in Fig. 3 (a). $\underline{\mu}^{(r)}$ and $\underline{\mu}^{(z)}$ are the relative complex permeabilities of a single conductor. To group conductors successfully in a winding segment they must have the same dimensions, the same material and they must be close together. When there is a cooling duct between two groups of conductors, it is advisable to group them in two separate segments. Fig. 3 shows how a set of conductors is grouped into a winding segment. Fig. 3(b) shows the approach used to define the size of the homogenized winding segment from the dimensions of the conductor arrangement and the corresponding homogenized permeability tensor $\underline{\tilde{\boldsymbol{\mu}}} = \text{diag}(\underline{\tilde{\mu}}^{(r)}, \underline{\tilde{\mu}}^{(z)})$. Fig. 3(a) and Fig. 3(b) also show the coordinates of the center of the conductors $(\rho_1, \rho_2, \cdots, \rho_i)$, which will be used later to determine the induced voltage in each conductor.

C. Equivalent magnetic model of the core

The core model uses basically the same principles as the conductor model (complex permeability + surface currents) in order to represent the frequency dependence of the losses in the magnetic steel. The difference is that there are no imposed external currents in the core. Considering this fact, the core can be represented by means a distribution of equivalent surface currents provided that the these surface currents satisfy the boundary equation (2), where in this case $\underline{\mu}^{(r)}$ and $\underline{\mu}^{(z)}$ stand for the complex permeabilities of the core.

The calculation of the complex permeabilities of the core is straightforward using the expressions (1) and (2) available in [16]. Once the complex permeabilities have been calculated, they are multiplied by stacking factor k_{fe} to obtain the effective complex permeability of the core. In the proposed model the core is represented by means of an arrangement of surface currents as shown in Figure 4.

D. Equivalent magnetic model of the transformer

The transformer is divided into g winding segments, which represent in an equivalent manner a group of conductors. Each winding segment is composed of an arrangement of surface currents and a volume current as shown in Fig. 4. On the other hand, the transformer core is represented by an array of surface currents as shown in Fig. 4. The transformer model is composed of three types of elements: *a.* Surface currents, *b.* volume currents and *c.* dummy elements.

a. Surface currents represent currents flowing close to the surface of the conductors. Surface currents are also used to represent the effect of the transformer core on the magnetic field. *b.* The *volume currents* represent the remaining current that does not flow near the surface of the conductor. Each winding segment has an accompanying volume current. *c. Dummy elements* are always located at the corners of the

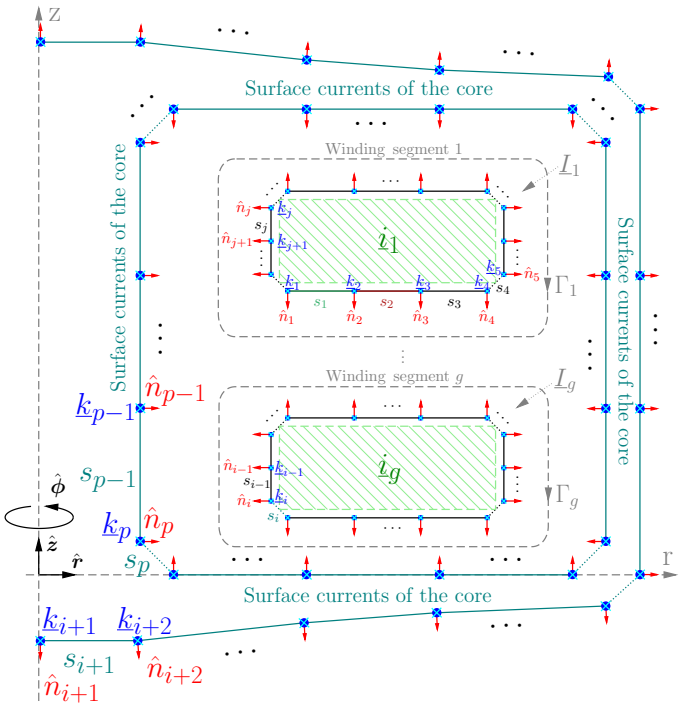

Fig. 4. General model layout. Segments size and corners have been exaggerated for better comprehension.

segments, they do not produce any magnetic field but they provide a very convenient way to obtain a consistent indexing of elements and field points. They also allow to avoid in a straightforward way the singularity that occurs at the corners of the rectangular segments. A dummy element is placed in the central axis of the core and also in each of its corners.

In addition to the elements, the transformer model also includes *field points* on which the boundary conditions are evaluated. There is a field point at each of the edges of each surface element. There is also a field point at the center of each conductor as shown in Fig. 3, which will be used later to calculate the induced voltages.

III. Mathematical Formulation of the Equivalent Magnetic Model of the Transformer

The main objective of this section will be to provide a mathematical formulation to calculate the magnetic vector potential in conductors. The magnetic vector potential in each conductor will be the fundamental piece for the calculation of each element of the impedance matrix.

A. Unknowns of the Model

As shown in Fig. 4, the variables for nodal surface current densities $\underline{k}_1 \cdots \underline{k}_p$ and volume currents $\underline{i}_1 \cdots \underline{i}_m$ are presented schematically. For example for an arbitrary surface element s_j the nodal surface current densities at its edges are k_j and k_{j+1}. The surface current density varies linearly from one edge to the other of each element allowing a smooth variation of the surface current along the surface of the core and winding segments [17]. The transformer model is composed of p surface elements in total. The first surface element is

s_1 which corresponds to a surface current belonging to the 1st winding segment, while the last surface element is s_p which corresponds to a dummy element belonging to the core as shown in Fig. 4. The numbering of surface elements and nodal surface current densities is assigned counterclockwise. An example of numbering in a case of two winding segments is shown in Fig. 12 of Appendix for better understanding. We define the vector $\mathbf{k}$ which contains the nodal surface current densities in A/m as follows

$$\mathbf{k} = \left[\underline{k}_1, \underline{k}_2, \cdots, \underline{k}_p\right]^T$$

$\mathbf{k}$ is a vector of size $p \times 1$. The volume currents represent the fraction of the current that does not flow on the conductor surface and are stored in the following vector

$$\mathbf{i} = \left[\underline{i}_1, \underline{i}_2, \cdots, \underline{i}_g\right]^T$$

$\mathbf{i}$ is a vector of size $g \times 1$. All the unknowns of the problem are arranged in the following column vector

$$\mathbf{x} = \left[\mathbf{k}; \mathbf{i}\right] \tag{6}$$

B. Known data of the model

Each winding segment is comprised of an arrangement of surface currents and a volume current. The total current (surface + volume) of the κ-th segment is denoted as $\underline{I}_\kappa$. The model is composed of g winding segments. This current is assumed to be known for all segments. The currents of the winding segments are stored in the vector $\mathbf{I}$

$$\mathbf{I} = \left[\underline{I}_1, \underline{I}_2, \cdots, \underline{I}_g\right]^T \tag{7}$$

C. Boundary Conditions

In the following sections an equation system will be formulated such that the following boundary conditions are fulfilled: *a.* Equation (2) must be satisfied at the boundary of the winding segments and at the boundary of the core with free space. *b.* The total current of a winding segment must satisfy the current specified in vector (7).

D. Magnetic Effects on Surface Elements

As shown in Fig. 4, each field point has a corresponding normal vector which can be written in terms of its radial and axial components, the normal vector related to the i-th field point is defined as $\hat{\boldsymbol{n}}_i = n_i^{(r)}\hat{\boldsymbol{r}} + n_i^{(z)}\hat{\boldsymbol{z}}$. The radial and axial components of normal vectors are stored in $\mathbf{n}_r$ and $\mathbf{n}_z$ respectively as follows

$$\mathbf{n}_r = \left[n_1^{(r)}, \cdots, n_p^{(r)}\right]^T, \mathbf{n}_z = \left[n_1^{(z)}, \cdots, n_p^{(z)}\right]^T \tag{8}$$

The magnetic field intensity produced by the j-th surface element on the i-th field point is defined as follows

$$\vec{\underline{\boldsymbol{H}}}_{i,j}^{(s)} = \left(a_{i,j}\underline{k}_j + a'_{i,j}\underline{k}_{j+1}\right)\hat{\boldsymbol{r}} + \left(b_{i,j}\underline{k}_j + b'_{i,j}\underline{k}_{j+1}\right)\hat{\boldsymbol{z}} \quad \text{for } j = 1\cdots p \text{ and } i = 1\cdots p \tag{9}$$

where $a_{i,j}$, $a'_{i,j}$, $b_{i,j}$ and $b'_{i,j}$ are called *geometric factors* as they only depend on the dimensions and location of the element that produces the field and on the coordinates of the field point. In general, geometric factors are real numbers and they can be calculated efficiently with mathematical formulations proposed in prior works [17], [18], [19]. All geometric factors related to Dummy elements are null because they do not contribute to the magnetic field, therefore $a_{i,d} = a'_{i,d} = b_{i,d} = b'_{i,d} := 0$ for $d \in \mathbb{D}\ \forall i$.

On the other hand, each volume current also produces a magnetic field on the field points of the surface elements, therefore we define the magnetic field intensity due to the j-th volume current on the i-th field point as follows

$$\vec{\underline{\boldsymbol{H}}}_{i,j}^{(c)} = c_{i,j}\underline{i}_j\hat{\boldsymbol{r}} + d_{i,j}\underline{i}_j\hat{\boldsymbol{z}} \text{ for } j = 1\cdots g \text{ and } i = 1\cdots p \tag{10}$$

where $c_{i,j}$ and $d_{i,j}$ are geometric factors which can be found using formulas for the magnetic field produced by a massive ring of rectangular cross section available in [20] section 3.3.3.

The surface currents are governed by the boundary condition (2), therefore for the particular case of i-th field point this expression can be written as follows

$$\hat{\boldsymbol{n}}_i \times \vec{\underline{\boldsymbol{H}}}_i = \mathbf{1}_2^T \cdot \left\{(\boldsymbol{\Upsilon}_i \cdot \boldsymbol{J}_2) \cdot \boldsymbol{\eta}_i^{\circ 2}\right\} \cdot \vec{\underline{\boldsymbol{K}}}_i \text{ for } i = 1\cdots p \tag{11}$$

where $\boldsymbol{\Upsilon}_i = \text{diag}(\underline{\gamma}_i^{(r)}, \underline{\gamma}_i^{(z)})$, $\underline{\gamma}_i^{(r)} = (1/2)(1 + \underline{\mu}_i^{(r)})/(1 - \underline{\mu}_i^{(r)})$, $\underline{\gamma}_i^{(z)} = (1/2)(1+\underline{\mu}_i^{(z)})/(1-\underline{\mu}_i^{(z)})$ and $\boldsymbol{\eta}_i = [n_i^{(r)}; n_i^{(z)}]$. For the sake of simplicity, we define

$$\underline{\gamma}_i := \mathbf{1}_2^T \cdot \left\{(\boldsymbol{\Upsilon}_i \cdot \boldsymbol{J}_2) \cdot \boldsymbol{\eta}_i^{\circ 2}\right\} \tag{12}$$

It should be noted that $\underline{\mu}_i^{(r)} := \underline{\tilde{\mu}}_\kappa^{(r)}$ and $\underline{\mu}_i^{(z)} := \underline{\tilde{\mu}}_\kappa^{(z)}\ \forall i \in \mathbb{K}_\kappa$ for $\kappa = 1\cdots g$ where $\underline{\tilde{\mu}}_\kappa^{(r)}$ and $\underline{\tilde{\mu}}_\kappa^{(z)}$ are calculated as indicated in section II-B. This work will consider that $\vec{\underline{\boldsymbol{H}}}_i$ and $\vec{\underline{\boldsymbol{K}}}_i$ are to be evaluated at the matching point between elements, therefore the surface current density of i-th element can be expressed as follows

$$\vec{\underline{\boldsymbol{K}}}_i = \underline{k}_i\hat{\boldsymbol{\phi}} \tag{13}$$

On the other hand, the total magnetic field on the i-th field point can be written as follows

$$\vec{\underline{\boldsymbol{H}}}_i = \sum_{j=1}^{p}\vec{\underline{\boldsymbol{H}}}_{i,j}^{(s)} + \sum_{j=1}^{g}\vec{\underline{\boldsymbol{H}}}_{i,j}^{(c)} = \sum_{j=1}^{p}\left\{\begin{array}{c}\left(a_{i,j}\underline{k}_j + a'_{i,j}\underline{k}_{j+1}\right)\hat{\boldsymbol{r}} \\ +\left(b_{i,j}\underline{k}_j + b'_{i,j}\underline{k}_{j+1}\right)\hat{\boldsymbol{z}}\end{array}\right\} + \sum_{j=1}^{g}\left\{c_{i,j}\underline{i}_j\hat{\boldsymbol{r}} + d_{i,j}\underline{i}_j\hat{\boldsymbol{z}}\right\} \text{ for } i = 1\cdots p \tag{14}$$

Combining (11), (13) and (14), performing the vector products between unit vectors and rearranging, the following expression is obtained

$$\hat{\boldsymbol{\phi}}\sum_{j=1}^{p}\left\{\begin{array}{c}\underline{k}_j\left(a_{i,j}n_i^{(z)} - b_{i,j}n_i^{(r)} - \underline{\gamma}_i\delta_{i,j}\right) \\ +\underline{k}_{j+1}\left(a'_{i,j}n_i^{(z)} - b'_{i,j}n_i^{(r)}\right)\end{array}\right\} + \hat{\boldsymbol{\phi}}\sum_{j=1}^{g}\left\{\underline{i}_j\left(c_{i,j}n_i^{(z)} - d_{i,j}n_i^{(r)}\right)\right\} = 0 \text{ for } i = 1\cdots p \tag{15}$$

where $\delta_{i,j}$ is the Kronecker delta function. Taking aside the unknown variables, the first sum in (15) can be written in matrix form as

$$\mathbf{F} = \left[\mathbf{a} \circ \left(\mathbf{n}_z \cdot \mathbf{1}_p^T\right) - \mathbf{b} \circ \left(\mathbf{n}_r \cdot \mathbf{1}_p^T\right) \mid \mathbf{0}_p\right] + \left[\mathbf{0}_p \mid \mathbf{a}' \circ \left(\mathbf{n}_z \cdot \mathbf{1}_p^T\right) - \mathbf{b}' \circ \left(\mathbf{n}_r \cdot \mathbf{1}_p^T\right)\right] \tag{16}$$

where the matrices $\mathbf{a} = (a_{i,j})_{p\times p}$, $\mathbf{a}' = (a'_{i,j})_{p\times p}$, $\mathbf{b} = (b_{i,j})_{p\times p}$, $\mathbf{b}' = (b'_{i,j})_{p\times p}$ store the geometric factors and $\mathbf{F} \in \mathbb{R}^{p\times p+1}$. $\mathbf{0}_p$ and $\mathbf{1}_p$ are zeros and ones column vectors of dimension $p\times 1$ respectively. $\circ$ denotes the Hadamard product (element-wise product) while $\cdot$ denotes the normal matrix product and the vertical bar denotes matrix concatenation. It should be noted that the material constants $\underline{\gamma}_i$ are still missing in (16) and will be included later in the equation system (23). The expression (16) will produce an additional $p+1$-th column in $\mathbf{F}$ related to $\underline{k}_{j+1}$ when $j = p$. The last column ($f_{*,p+1}$) of $\mathbf{F}$ is discarded and the result is assigned to the *surface interaction matrix* $\mathbf{M}_s$. This is denoted as $\mathbf{M}_s = \mathbf{F}^{-}_{*,p+1}$. Matrix $\mathbf{M}_s \in \mathbb{R}^{p\times p}$ represents all the magnetic effects produced by the surface elements between and on themselves.

On the other hand, the second sum in (15) can be written in matrix form as follows

$$\mathbf{M}_c = \mathbf{c} \circ \left(\mathbf{n}_z \cdot \mathbf{1}_g^T\right) - \mathbf{d} \circ \left(\mathbf{n}_r \cdot \mathbf{1}_g^T\right) \tag{17}$$

where $\mathbf{c} = (c_{i,j})_{p\times g}$ and $\mathbf{d} = (d_{i,j})_{p\times g}$. Matrix $\mathbf{M}_c \in \mathbb{R}^{p\times g}$ represents all the magnetic effects of volume currents on surface elements.

E. Total current in winding segments

Each winding segment must satisfy Ampere's law, therefore the following relationship must hold for the κ-th segment

$$\oint_{\Gamma_\kappa} \underline{\vec{\boldsymbol{H}}} \cdot \mathrm{d}\vec{\boldsymbol{l}} = \underline{I}_\kappa \text{ for } \kappa = 1\cdots g \tag{18}$$

These relationships also imply that the total current enclosed by the amperian contour must be equal to the segment current. Considering that the surface elements have a linear surface current distribution, it can be shown that the current of the j-th surface element can be calculated as follows

$$\underline{i}_j^{(s)} = l_j \frac{\underline{k}_j + \underline{k}_{j+1}}{2} \text{ where } j \in \mathbb{K}_\kappa \text{ and } \kappa = 1\cdots g \tag{19}$$

where l_j is the length of j-th surface element, $\mathbb{K} = \{1, 2, \cdots, p\}$ is the set with the indexes of the surface elements and $\mathbb{K}_\kappa$ (where $\mathbb{K}_\kappa \subset \mathbb{K}$) is the subset of surface elements in segment κ. The total current of the κ-th segment can be written as follows

$$\underline{I}_\kappa = \underline{i}_\kappa + \sum_{j\in\mathbb{K}_\kappa} \underline{i}_j^{(s)} \text{ for } \kappa = 1\cdots g \tag{20}$$

It should be noticed that $\mathbb{K}$ have $g+1$ valid subsets where the subset $\mathbb{K}_{g+1}$ is reserved for the indexes of surface elements belonging to the core.

Remembering that dummy elements do not contribute to the magnetic field and their length in practical terms is close to zero, we define $\mathbb{D}$ (where $\mathbb{D} \subset \mathbb{K}$) as the set of dummy elements indexes, this leads to $l_d := 0 \Rightarrow \underline{i}_d^{(s)} = 0 \ \forall\ d \in \mathbb{D}$. Introducing (19) in (20) and rearranging

$$\sum_{j\in\mathbb{K}_\kappa} \left(l_j\underline{k}_j + l_j\underline{k}_{j+1}\right) + 2\underline{i}_\kappa = 2\underline{I}_\kappa \text{ for } \kappa = 1\cdots g \tag{21}$$

Writing (21) in matrix form

$$\boldsymbol{\ell} \cdot \mathbf{k} + 2 \cdot \boldsymbol{I}_g \cdot \mathbf{i} = 2 \cdot \mathbf{I} \tag{22}$$

where $\boldsymbol{\ell}$ is a matrix of dimension $g \times p$ which contains the lengths of all surface elements. The lengths of the elements belonging to winding segments are arranged consistently with expression (21). $\boldsymbol{I}_g$ is the identity matrix of size $g\times g$. It should be noticed that in the context of expression (22) the surface elements of the core shall not be taken into consideration, therefore it is defined $l_j := 0 \ \forall\ j \in \mathbb{K}_{g+1}$. This means that the elements of the core must not meet any special condition with regard to the total current.

F. Equation System Formulation

Assembling equations (16), (17) and (22) the following linear system of equations is obtained

$$\begin{bmatrix} \mathbf{M}_s - \boldsymbol{\gamma} & \mathbf{M}_c \\ \boldsymbol{\ell} & 2\cdot\boldsymbol{I}_g \end{bmatrix} \cdot \begin{bmatrix} \mathbf{k} \\ \mathbf{i} \end{bmatrix} = \begin{bmatrix} \mathbf{0}_p \\ 2\cdot\mathbf{I} \end{bmatrix} \tag{23}$$

where $\boldsymbol{\gamma}$ stores the material constants in a diagonal matrix defined as $\boldsymbol{\gamma} = \mathrm{diag}(\underline{\gamma}_1, \cdots, \underline{\gamma}_p)$. Notice that at least one element of $\mathbf{I}$ must be non-zero to obtain a non-trivial solution. In compact form the system is as follows

$$\mathbf{M}_{sys} \cdot \mathbf{x} = \mathbf{b}_{sys} \tag{24}$$

Since the system (24) is to be solved m times for a given frequency, it is more convenient to obtain its solution as $\mathbf{x} = \mathbf{M}_{sys}^{-1} \cdot \mathbf{b}_{sys}$. It is true that the calculation of the inverse matrix has a higher computational cost than solving a linear system of equations, however the advantage of solving the problem this way is that the inverse is computed once at a given frequency and then is reused m times for the different states of vector $\mathbf{b}_{sys}$. This strategy produces a significant reduction in total computation time especially when m is large, which is usually observed in power transformer modeling.

G. Calculation of the magnetic vector potential in conductors

As will be seen in the next section, the magnetic vector potential in the conductors will be required for the calculation of the voltage in the conductors. Once the equations system (23) has been solved, the nodal surface current densities $\mathbf{k}$ and the volume currents of winding segments $\mathbf{i}$ are available. Consider the diagram in Fig. 3 (a). A field point has been placed at the center point of each conductor denoted as ρ_i for $i = 1\cdots q$ where q is the total number of actual conductors. The total magnetic vector potential in the i-th conductor $\underline{\vec{\boldsymbol{A}}}_i = \underline{A}_i\hat{\boldsymbol{\phi}}$ is composed by the contributions of the surface and volume currents. The magnetic vector potential produced by j-th volume current on the i-th field point can be expressed as follows

$$\underline{A}_{i,j}^{(c)} = e_{i,j}\underline{i}_j \text{ for } j = 1\cdots g \text{ and } i = 1\cdots q \tag{25}$$

where $e_{i,j}$ is the magnetic vector potential geometric factor produced by a volume current in a field point and it can be calculated as described in [20] section 3.3.3. Similarly the magnetic vector potential produced by the j-th surface element on the i-th field point

$$\underline{A}_{i,j}^{(s)} = o_{i,j}\underline{k}_j + o'_{i,j}\underline{k}_{j+1} \text{ for } j = 1\cdots p \text{ and } i = 1\cdots q \tag{26}$$

where $o_{i,j}$ and $o'_{i,j}$ are magnetic vector potential geometric factors produced by a surface current in a field point and they can be calculated as described in [17], [18], [19]. Therefore the magnetic vector potential at the center of the conductor i-th conductor is

$$\underline{A}_i = \sum_{j=1}^{p} \left(o_{i,j}\underline{k}_j + o'_{i,j}\underline{k}_{j+1}\right) + \sum_{j=1}^{g} \left(e_{i,j}\underline{i}_j\right) \text{ for } i = 1 \cdots q \tag{27}$$

The matrix $\mathbf{O}$ is defined as $\mathbf{O} = \left[\mathbf{o} \mid \mathbf{0}_q\right] + \left[\mathbf{0}_q \mid \mathbf{o}'\right]$ where the matrices $\mathbf{o} = (o_{i,j})_{q\times p}$, $\mathbf{o}' = (o'_{i,j})_{q\times p}$ store the geometric factors between surface currents and field points. The magnetic vector potential at the center of each conductor can be calculated using the following matrix expression

$$\mathbf{A} = \left(\mathbf{O}^{-}_{*,p+1}\right) \cdot \mathbf{k} + \mathbf{e} \cdot \mathbf{i} \tag{28}$$

where the matrix $\mathbf{e} = (e_{i,j})_{q\times g}$ stores the geometric factors between volume currents and field points, $\mathbf{O}^{-}_{*,p+1}$ is equal to matrix $\mathbf{O}$ but discarding the last column and $\mathbf{A}$ is a column vector of size $q \times 1$ which stores magnetic vector potential at the center point of each conductor.

IV. Calculation of the Impedance Matrix

This section will present the methodology for the calculation of the impedance matrix from the magnetic solution obtained in the previous section.

A. Voltage in branches

The induced voltage in a conductor is given by $\underline{v} = \underline{j}2\pi r\omega\underline{A}$, therefore it can be written in a general form for all the conductors

$$\mathbf{v} = \underline{j}4\pi^2 f \cdot \mathbf{r} \circ \mathbf{A} \tag{29}$$

where $\mathbf{r} = [r_1, \cdots, r_q]^T$ is a column vector that stores the mean radii of all conductors and f is a given frequency. Let's define $\mathbb{S} = \{1, 2, \cdots, g\}$ as the set with the indexes of winding segments and $\mathbb{S}_\tau$ (where $\mathbb{S}_\tau \subset \mathbb{S}$) is the subset of segments in branch τ for $\tau = 1, 2, \cdots, m$. We also define $\mathbb{W} = \{1, 2, \cdots, q\}$ as the set with the indexes of the conductors and $\mathbb{W}_\kappa$ (where $\mathbb{W}_\kappa \subset \mathbb{W}$) is the subset of conductors in winding segment κ for $\kappa = 1, 2, \cdots g$. For the purpose of impedance matrix calculation, 1 A is injected in one branch and 0 A in the rest of the branches. It is assumed that all conductors in a branch have the same current. Therefore, the voltage of a branch is the sum of the voltages of the conductors belonging to the segments of that branch.

$$\underline{V}_\tau = \sum_{j\in\mathbb{S}_\tau} \sum_{i\in\mathbb{W}_j} \underline{v}_i \text{ for } \tau = 1 \cdots m \tag{30}$$

In matrix form the branch voltages are stored as follows $\mathbf{V} = [\underline{V}_1, \cdots, \underline{V}_m]^T$. Similarly, the branch currents are stored in the vector $\mathbf{I}^{(b)} = [\underline{I}_1^{(b)}, \cdots, \underline{I}_m^{(b)}]^T$ while $\mathbf{N} = [N_1, \cdots, N_m]^T$ is the vector containing the number of parallel conductors per turn of each branch.

B. Methodology for the calculation of the impedance matrix at a set of frequencies

Considering that the resistive and inductive elements of the impedance matrix have a relatively smooth variation with frequency, this allows for a discrete sweep over a specific set of selected frequencies. We define the frequency set as $\mathbf{f} = \{f_1, f_2, \cdots, f_{n_f}\}$. The impedance matrix is then defined as $\mathbf{Z} = (\underline{Z}_{i,j,k})_{m\times m\times n_f}$. The methodology for the calculation the impedance matrix is presented in Algorithm 1. It is important to make a remark about the solution of the equation system for each state of the vector $\mathbf{b}_{sys}$. In general, for each state of vector $\mathbf{b}_{sys}$ one should solve the matrix product $\mathbf{M}_{sys}^{-1} \cdot \mathbf{b}_{sys}$, however one can take advantage of the strong sparsity of vector $\mathbf{b}_{sys}$. Instead of performing the product of a dense matrix by a sparse vector, it can be shown that the solution of the equation system for the j-th state of the vector $\mathbf{b}_{sys}$ can be computed as $\sum_{\varkappa\in\mathbb{S}_j} [2 \cdot \mathbf{G}_{*,p+\varkappa} \cdot n(\mathbb{W}_\varkappa)]$ where $n(\mathbb{W}_\varkappa)$ denotes the cardinality of the subset $\mathbb{W}_\varkappa$. This can be seen in line 15 of Algorithm 1. Once the impedance matrix has been obtained, the self-resistance and self-inductance components (R_s and L_s) are to be added to the diagonal elements as described in [9].

Algorithm 1 Proposed methodology for $\mathbf{Z}$ calculation

1: Discretize using surface elements and volume currents.
2: Assign indexes to elements. Populate: $\mathbb{K}, \mathbb{K}_\kappa, \mathbb{D}$
3: Group conductors into segments. Populate $\mathbb{W}, \mathbb{W}_\kappa$
4: Group winding segments into branches. Populate $\mathbb{S}, \mathbb{S}_\tau$
5: Populate: $\mathbf{n}_r, \mathbf{n}_z, \boldsymbol{\ell}, \mathbf{r}$
6: Calc. matrices: $\mathbf{a}, \mathbf{a}', \mathbf{b}, \mathbf{b}', \mathbf{c}, \mathbf{d}, \mathbf{e}, \mathbf{o}, \mathbf{o}'$
7: Calc. matrices: , $\mathbf{F}, \mathbf{M}_s, \mathbf{M}_c, \mathbf{O}$
8: **for** $k \leftarrow 1$ to n_f **do**
9: $f \leftarrow f_k$
10: Calc. complex permeabilities @ f
11: Update matrices: $\boldsymbol{\gamma}, \mathbf{M}_{sys}$
12: $\mathbf{G} \leftarrow \mathbf{M}_{sys}^{-1}$ ▷ Compute inverse matrix
13: **for** $j \leftarrow 1$ to m **do**
14: $\underline{I}_*^{(b)} \leftarrow 0$; $\underline{I}_j^{(b)} \leftarrow 1$ ▷ Set branch currents
15: $[\mathbf{k}; \mathbf{i}] \leftarrow \sum_{\varkappa\in\mathbb{S}_j} [2 \cdot \mathbf{G}_{*,p+\varkappa} \cdot n(\mathbb{W}_\varkappa)]$
16: Calc. conductor vector pot. $\mathbf{A}$ using (28)
17: Calc. conductor voltages $\mathbf{v}$ using (29)
18: Calc. branch voltages $\mathbf{V}$ using (30)
19: **for** $i \leftarrow 1$ to m **do**
20: $\underline{Z} \leftarrow \underline{V}_i \div \underline{I}_j^{(b)}$
21: $\underline{Z}_{i,j,k} \leftarrow \underline{Z} \div N_j^2$
22: **end for**
23: **end for**
24: **end for**

V. Results and Validation

A. Description of the case study

The case study is a 50 MVA single-phase transformer with rated voltages $230/\sqrt{3}$, $69/\sqrt{3}$, 13.8 kV at 60 Hz manufactured by WEG in Mexico. The winding arrangement is composed of three main windings (LV, TV and HV) plus a

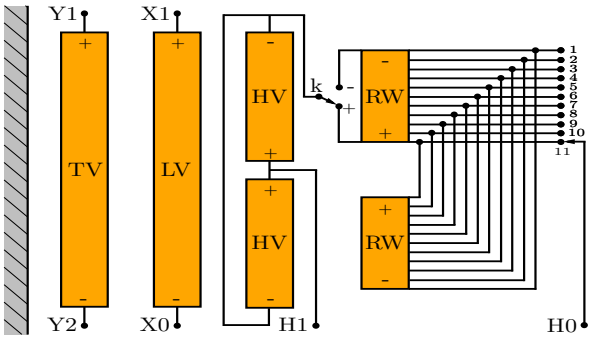

Fig. 5. Single phase transformer connection diagram. The positions of selector k and tap for H0 are indicative and may change according to the connection configuration.

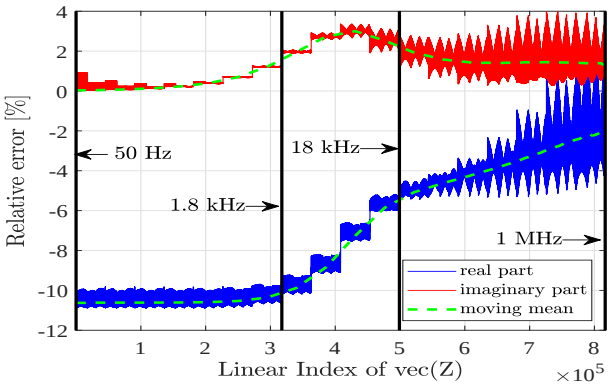

Fig. 7. Relative error of the impedance matrix calculated with the proposed methodology compared to the finite element calculation.

regulating winding (RW) as shown in Fig. 5. Detailed information on this transformer can be found in [21]. This transformer has been the subject of a extensive measurement campaign by the CIGRE JWG A2/C4.52 with the aim of evaluating the accuracy of various high-frequency models. The most relevant information regarding the tests and measurements performed in the case study is available in [22]. The detailed design information and data of transient measurements are available at [21].

B. Calculation of the impedance matrix for the case study

For the calculation of the impedance matrix, the transformer conductors were grouped into 213 branches. The discretization of the top winding assembly using surface elements is presented in Fig. 6(a). As can be seen, the proposed method

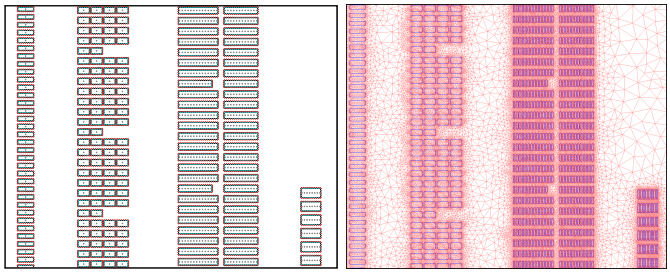

Fig. 6. Discretization of the top winding assembly of the case study by means of the proposed methodology [left panel] (a) and FEM [right panel] (b).

is a mesh-free model which means that neither the air nor the interior of the winding segments need to be subdivided with elements. Inside the winding segments the center of each conductor is marked by an 'x' as shown in Fig. 3. It is at these points where the magnetic vector potential is calculated.

With regard to frequency, a logarithmic sweep of 4 frequencies per decade was considered, obtaining the following set of frequencies $\mathbf{f} = \{\ 0.05,\ 0.1,\ 0.18,\ 0.32,\ 0.56,\ 1,\ 1.8,\ 3.2,\ 5.6,\ 10,\ 18,\ 32,\ 56,\ 100,\ 180,\ 320,\ 560,\ 1000\ \} \times 10^3$ Hz for a total of 18 frequencies. The impedance matrix was computed using Algorithm 1 which led to a complex matrix ($\mathbf{Z}_{prop}$) of size $213 \times 213 \times 18$.

Furthermore, the impedance matrix was also calculated with FEM ($\mathbf{Z}_{fem}$) using FEMM software [23] by applying 1 A to each branch at a time and then the voltage in all branches was determined. This process required a total of 3834 FEMM program runs. The model implemented in FEM is exactly the same as the one used in [3] and [5] with the aim of replicating the same impedance matrix and the same results of those transient studies. The only difference in the FEM calculations performed here with respect to [3] and [5] is that in this work the calculations were performed on a single 4 Ghz Core i7 - 32 GB RAM computer.

The FEM discretization of the top winding assembly is presented in Fig. 6(b). In the FEM model the air, the core and the interior of the conductors are to be discretized with triangular elements. This mesh was kept fixed at all simulated frequencies.

C. Direct comparison of impedance matrices

Once the impedance matrices have been calculated the relative error was calculated between them as $\mathbf{Err} = (\mathbf{Z}_{prop} - \mathbf{Z}_{fem}) \oslash \mathbf{Z}_{fem}$ where $\oslash$ is the symbol of Hadamard's division. Considering that the impedance matrix is complex and three-dimensional, the vectorized form of **Err** has been used to visualize the global behavior of the relative error between $\mathbf{Z}_{prop}$ and $\mathbf{Z}_{fem}$. Fig. 7 shows the relative error between proposed method and finite element method for the real and imaginary part of the impedance matrix. The linear index of each position of the impedance matrix has been placed on the horizontal axis which starts at 1 and ends at $816642\ (213 \cdot 213 \cdot 18)$.

As can be seen, the real part of the impedance is the one with the highest relative error variations. It is interesting to note that the relative error of the real part is higher at low frequency (about -10 % up to 1800 Hz), and starts to decrease as the frequency increases. It can also be observed that although the error decreases as the frequency increases, its dispersion becomes larger with respect to the FEM calculations.

D. Calculation of transient responses in the time domain

In order to evaluate the ability of the proposed methodology to produce impedance matrices suitable for the calculation of high frequency transients, two equivalent state-space models of the case study have been created, one using the impedance

matrix calculated with FEM and the other using the impedance matrix calculated with the proposed method. The methodology used to obtain the state space models of the case study was exactly the same as proposed in [3] which was summarized in steps *a* through *e* in the introduction of this paper. In this work the transients were calculated using the ODE45 solver of Matlab which implements the Runge-Kutta method for the solution of the system of differential equations. Alternatively, any EMTP software that supports the usage of state-space models such as EMTP-RV or PSCAD can also be used.

The case study transformer has been intensively analyzed in the time domain within the framework of the JWG CIGRE A2/C4.52 group. As a result of this measurement campaign, time domain measurements of 64 different connection configurations are available. The input voltage in all cases was a standard lightning impulse of 1.2/50 μs at one of the transformer terminals. Details on the measurements are available in [22]. In this work, configurations number 6, 26, 42 and 54 were considered. The connections of each configuration are described below:

Configuration 6: X0, H0 grounded; Y1, Y2, X1 open; impulse applied to H1. Selector k in positive position. H0 connected to tap 11. *Configuration 26*: X0, H1 grounded; Y1, Y2, X1 open; impulse applied to H0. Selector k in negative position. H0 connected to tap 1. *Configuration 42*: X0, H0 grounded; Y1, Y2, H1 open; impulse applied to X1. Selector k in negative position. H0 connected to tap 1. *Configuration 54*: X1, H0 grounded; Y1, Y2, H1 open; impulse applied to X0. Selector k in positive position. H0 connected to tap 11.

Figs. 8, 9, 10 and 11 show the measured and calculated voltages using the impedance matrix obtained with FEM and with the proposed methodology for various configurations. A good agreement was found between measurements and calculations, and it can be seen an excellent agreement between the results obtained with FEM and with the proposed methodology.

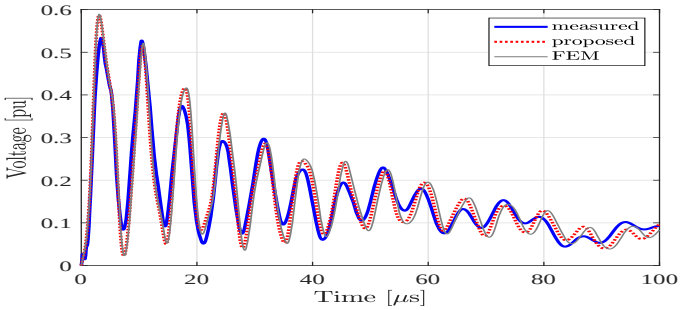

Fig. 8. Transient voltages at terminal X1, input on H1 for case 6.

VI. Discussion

Table I provides a summary of the computation time used by the proposed method in various tasks related to the computation of the impedance matrix. As can be seen, the proposed method uses a significant amount of time (about 15%) in the calculation of the geometric factors and in the assembly of various matrices necessary for subsequent calculations. Once these matrices have been obtained, they are available to update the system matrix and to calculate the magnetic vector potential in the conductors at each of the selected frequencies. The remaining computation time (about 85%) is spent on the solution of the equation system by means of the inverse matrix calculation. On the other hand, in Table II the FEM times for the calculation of the impedance matrix are also reported. In this case it can be seen that about 93% of the calculation time is used in the solution of the equation system. Table III presents the overall performance summary of FEM and the proposed method, noting that FEM has required a slightly more than one million elements to discretize the geometry of the problem, which produces an equation system of about half a million degrees of freedom. Although the equation system produced by FEM is sparse, it is a large system that is to be solved multiple times. This explains why most of the FEM computation time is spent solving the equation system.

Table III also shows a significant reduction in the total calculation time using the proposed method compared to FEM. The proposed method has taken about 11 hours to complete the impedance matrix calculation, while FEM has taken a

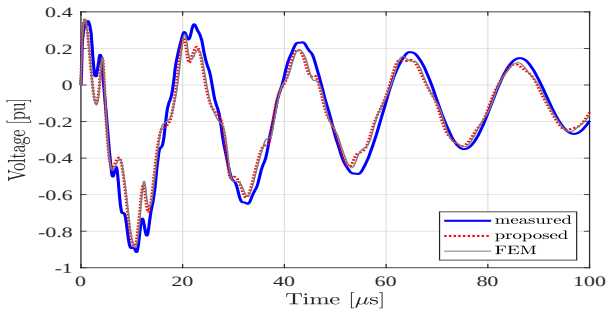

Fig. 9. Transient voltages at terminal X1, input on H0 for case 26.

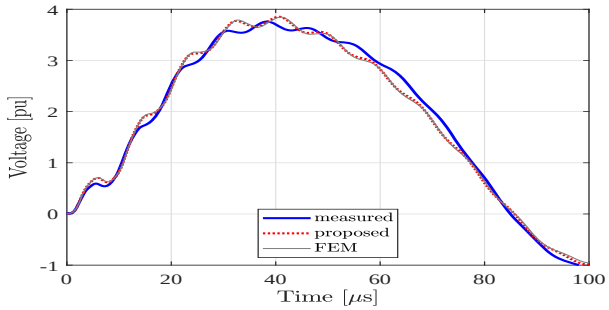

Fig. 10. Transient voltages at terminal H1, input on X1 for case 42.

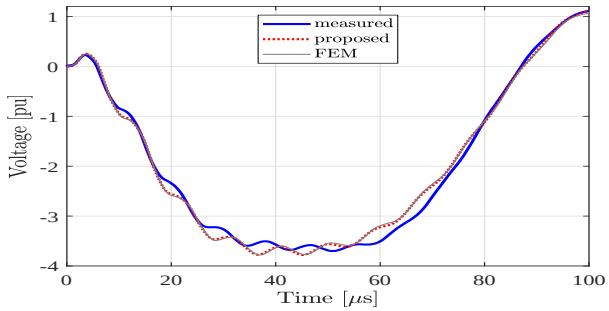

Fig. 11. Transient voltages at terminal H1, input on X0 for case 54.

slightly more than 3 weeks. It is important to give a proper interpretation to these results because in the case of FEM the calculation time can be influenced by the software used and in turn by the possibility of using advanced features such as adaptive meshing, mesh reusing or direct access to the equation system. To obtain the impedance matrix with FEM, the classical methodology described in [4] in section 13.10.3 has been implemented using the FEMM software. A special effort has been made to make the FEMM execution as efficient as possible within the possibilities offered by the Matlab-FEMM communication interface and some strategies have been applied to speed up the program execution such as the reuse of the problem geometry and the efficient assignment of currents and material properties. As a consequence of these optimizations, it can be seen in Table II that less than 2 % of the total computation time is spent on these tasks. Most of the computation time spent by FEM is spent on the solution of the equation system.

On the other hand, the proposed methodology has a series of features that together make it possible to calculate the impedance matrix in a considerably shorter calculation time compared to FEM. Among these attributes we can mention the following:

a. This is a mesh-free method. This avoids the discretization of air, core interior and conductors. As a consequence, the proposed method produces an equation system about 19 times smaller than the one obtained with FEM. Although the equation system produced by the proposed method is strongly dense because the mathematical formulation is of integral type, this equation system can be handled without inconveniences by means of the use of virtual memory if necessary.

b. The most important strength that gives the proposed methodology an important advantage over FEM is the reuse of calculations. This reuse is performed at two levels. In the first level, the geometric factors $\mathbf{a}, \mathbf{a}', \mathbf{b}, \mathbf{b}', \mathbf{c}, \mathbf{d}, \mathbf{e}, \mathbf{o}, \mathbf{o}'$ are calculated. With these geometric factors the matrices $\mathbf{M}_s$, $\mathbf{M}_c$ and $\mathbf{O}$ are built. These three matrices are kept fixed and are reused at each of the simulation frequencies. At a second level, the inverse of the system matrix at a given frequency is calculated. The columns of this matrix are used to directly obtain the solution of the volume and surface currents for the m states of the vector $\mathbf{b}_{sys}$.

This means that for the case study transformer analysis, a single $\mathbf{M}_{sys}$ matrix inversion would be equivalent to solving 213 equation systems in FEM. As a result, the proposed method solves a total of 18 system matrix inversions, while FEM must solve 3834 systems of equations.

In addition, the memory consumption of both methods is also presented in Table III. The most memory-demanding step of the proposed method is the assembly of matrix $\mathbf{F}$ since all the matrices in (16) are dense and cannot be stored as sparse matrices. In case of memory limitations matrix $\mathbf{F}$ can be assembled in a sequence of steps to avoid having all the matrices in memory at the same time or one can also resort to the use of virtual memory stored in a solid state disk (SSD).

Another aspect that is important to highlight is the excellent agreement of the time domain transient responses presented in Figs 8, 9, 10 and 11 between the results calculated using the FEM impedance matrix and that obtained with the proposed method.

TABLE I
CALCULATION TIMES OF THE PROPOSED METHOD.
HARDWARE: 4 GHZ CORE I7 - 32 GB RAM COMPUTER

Type of computation	Time (s)	% of TST
Geometric factors $\mathbf{a}$, $\mathbf{b}$, $\mathbf{a}'$, $\mathbf{b}'$	4558.8	12.34
Geometric factors $\mathbf{c}$, $\mathbf{d}$	435.4	1.18
Geometric factors $\mathbf{o}$, $\mathbf{o}'$, $\mathbf{e}$	293.3	0.79
Matrix assembly $\mathbf{M}_s$, $\mathbf{M}_c$, $\mathbf{O}$	206.6	0.56
Solution of the eq. system (Mat. Inv.)	31107.6	84.18
$\mathbf{A}$, $\mathbf{V}$, $\mathbf{Z}$ calculation	351.8	0.95
Total simulation time (TST)	**36953.5**	100

TABLE II
CALCULATION TIMES OF FEM.
HARDWARE: 4 GHZ CORE I7 - 32 GB RAM COMPUTER

Type of computation	Time (s)	% of TST
Set mat. prop. & curr. Meshing	24125.8	1.02
Solution of the eq. system	2211067.1	93.28
Calculation of induced voltages	135107.4	5.70
Total simulation time (TST)	**2370300.3**	100

TABLE III
PERFORMANCE COMPARISON BETWEEN FEM AND PROPOSED METHOD

	No. of Elements	No. of Unknowns	No. of Eq. Sys. Solved	Sim. Time	Mem. Max.
FEM	1105715	553217	3834	658.4 h	572.4 MB
Proposed	29134	29134	18	10.3 h	31.8 GB

A direct comparison of the impedance matrices calculated with FEM and with the proposed method shows that the most significant errors occur at relatively low frequencies. On the other hand Fig. 7 also shows that the relative error between the impedance matrices tends to reduce from 18 kHz onwards. This trend is convenient since the behavior of the model at medium and high frequency is the one that determines to a greater extent the transient response to high frequency disturbances such as atmospheric discharges and switching in the power system.

Although good agreement was found between the proposed method and FEM, there are still some discrepancies between simulations and transient measurements that may be attributed to following factors: *a.* Frequency dependence of capacitances. *b.* Magnetic effects related to the three-dimensionality of the core. Considering the magnitude and complexity of these topics, they may be the subject of future research projects.

VII. CONCLUSIONS

In this work a new methodology has been proposed for the fast calculation of the impedance matrix of power transformers. The main outcome of this work is that the proposed methodology makes available to the industry the possibility of creating models for the calculation of electromagnetic transients (including resonant transients) in a calculation time compatible with the internal processes of power transformer manufacturers. This will allow

the strengthening of cooperative relationships between manufacturers and purchasers to assess the performance of the transformer under disturbances that may occur in the power network even before the unit is manufactured, allowing timely measures to be adopted, either in the design or in the operating protocols to aim for a safer operation of the transformer and consequently of the power network.

The proposed model incorporates the frequency dependence of the impedances representing the core and coils which allows an adequate modeling of the losses and consequently of the damping in the resulting white-box model of the power transformer. The proposed methodology has been successfully validated on a real 50 MVA transformer by calculating the transient response for different connection configurations. These results have shown that the proposed methodology is appropriate to produce impedance matrices suitable for high frequency transient calculations in power transformers.

VIII. Appendix

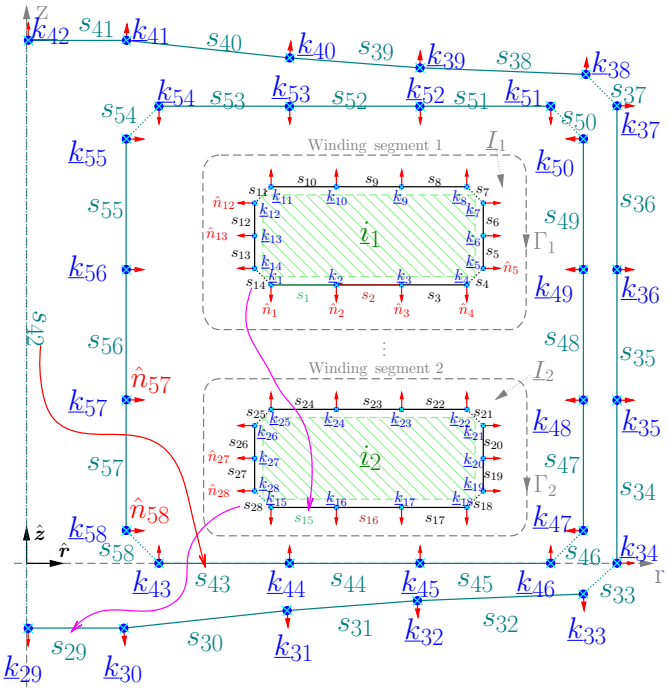

Fig. 12. Example of numbering in a simple case, s_{42} is a dummy element.

IX. Acknowledgements

The authors wish to extend our thanks to Álvaro Portillo and Bjørn Gustavsen for their support and many fruitful discussions on transformer modeling in the last years working together in the JWG CIGRE A2/C4.52.

References

[1] J. A2/C4.39, "Electrical transient interaction between transformers and the power system. part 1. expertise," *CIGRE Tech. Brochure 577A*, 2014.

[2] ——, "Electrical transient interaction between transformers and the power system. part 2. case studies," *CIGRE Tech. Brochure 577B*, 2014.

[3] E. E. Mombello, A. Portillo, and G. A. D. Florez, "New state-space white-box transformer model for the calculation of electromagnetic transients," *IEEE Transactions on Power Delivery*, vol. 36, no. 5, pp. 2615–2624, 2021.

[4] S. V. Kulkarni and Khaparde, *Transformer engineering: design, technology, and diagnostics 2nd Ed.* CRC press, 2013.

[5] E. E. Mombello and G. A. Diaz Florez, "An improved high frequency white-box lossy transformer model for the calculation of power systems electromagnetic transients," *Electric Power Systems Research*, vol. 190, p. 106838, 2021.

[6] D. Wilcox, W. Hurley, and M. Conlon, "Calculation of self and mutual impedances between sections of transformer windings," *Generation, Transmission and Distribution, IEE Proceedings C*, vol. 136, pp. 308 – 314, 10 1989.

[7] F. de Leon and A. Semlyen, "Efficient calculation of elementary parameters of transformers," *IEEE Transactions on Power Delivery*, vol. 7, no. 1, pp. 376–383, 1992.

[8] ——, "Detailed modeling of eddy current effects for transformer transients," *IEEE Transactions on Power Delivery*, vol. 9, no. 2, pp. 1143–1150, 1994.

[9] O. Moreau, L. Popiel, and J. Pages, "Proximity losses computation with a 2d complex permeability modelling," *IEEE Transactions on Magnetics*, vol. 34, no. 5, pp. 3616–3619, 1998.

[10] E. Bjerkan and H. Hoidalen, "High frequency fem-based power transformer modeling: Investigation of internal stresses due to network-initiated overvoltages," *Electric Power Systems Research*, vol. 77, no. 11, pp. 1483–1489, 2007, selected Topics in Power System Transients - Part II.

[11] E. Bjerkan, "High frequency modeling of power transformers. stresses and diagnostics," *Ph.D. thesis*, 2005.

[12] X. M. Lopez-Fernandez, H. Rodriguez-Ignacio, and C. Alvarez-Marino, "Hf-dependent parameter calculation by fem for power transformer," in *2017 18th International Symposium on Electromagnetic Fields in Mechatronics, Electrical and Electronic Engineering (ISEF)*, 2017, pp. 1–2.

[13] N. Abeywickrama, Y. V. Serdyuk, and S. M. Gubanski, "High-frequency modeling of power transformers for use in frequency response analysis (fra)," *IEEE Transactions on Power Delivery*, vol. 23, no. 4, pp. 2042–2049, 2008.

[14] G. Diaz and E. Mombello, "Semianalytic integral method for fast solution of current distribution in foil winding transformers," *Magnetics, IEEE Transactions on*, vol. 51, no. 9, pp. 1–9, Sept 2015.

[15] Á. Portillo, L. F. de Oliveira, and F. Portillo, "Calculation of circuit parameters of high frequency models for power transformers using fem," in *5th International Colloquium on Transformer Research and Asset Management*. Springer, 2020, pp. 163–182.

[16] K. G. N. B. Abeywickrama, A. D. Podoltsev, Y. V. Serdyuk, and S. M. Gubanski, "Influence of core characteristics on inductance calculations for modeling of power transformers," in *First International Conference on Industrial and Information Systems*, 2006, pp. 24–29.

[17] G. Diaz, E. Mombello, and S. Voss, "Mathematical formulation of a new linear surface element for the modeling of axisymmetric magnetic field problems," *International Journal of Applied Electromagnetics and Mechanics*, vol. 61, no. 2, pp. 273–292, 2019.

[18] G. Diaz and E. Mombello, "Magnetic field due to a finite current carrying disk considering a variable current density along its radial dimension," *International Journal of Applied Electromagnetics and Mechanics*, vol. 42, no. 1, pp. 119–136, 2013.

[19] ——, "New compact and singularity free formulations for the magnetic field produced by a finite cylinder considering linearly varying current density," *International Journal of Applied Electromagnetics and Mechanics*, vol. 50, no. 2, pp. 483–501, 2016.

[20] I. Dolezel, P. Karban, and P. Solin, *Integral methods in low-frequency electromagnetics*. John Wiley & Sons, 2009.

[21] G. Diaz, E. E. Mombello, J. J. Perez, and H. K. Hoidalen, "50 MVA single-phase power transformer design data and measurements." *IEEE Dataport*, 2022. [Online]. Available: https://dx.doi.org/10.21227/b9qq-nq89

[22] B. Gustavsen, A. Portillo, R. Ronchi, and A. Mjelve, "Measurements for validation of manufacturers white-box transformer models," *Procedia Engineering*, vol. 202, pp. 240–250, 2017, special issue of the 4th International Colloquium "Transformer Research and Asset Management".

[23] D. Meeker, "Finite element method magnetics v. 4.2," *FEMM*, 2019.